DOI: 10.1002/ejic.200601052

Theoretical Studies of the Electronic Structure and Spectroscopic Properties of $[Ru(Htcterpy)(NCS)_3]^{3-}$

Ming-Xia Li,[a,b] Hong-Xing Zhang,*[a] Xin Zhou,[a] Qing-Jiang Pan,[b] Hong-Gang Fu,[b] and Chia-Chung Sun[a]

Keywords: Black dyes / Electronic structure / Spectroscopic properties / Solvent effects

The ground- and excited-state structures of $[Ru(Htcterpy)(NCS)_3]^{3-}$ (**1H**) (tcterpy = 4,4′,4′′-tricarboxy-2,2′:6′,2′′-terpyridine) are optimized by the DFT and CIS methods, respectively. Absorption and emission spectra in the gas phase and in solution (ethanol and water) are predicted at the TD-DFT/B3LYP level. Experimental spectra are roughly reproduced by our calculated results. In ethanol solution, the HOMOs of the absorption spectra are dominated by d orbitals of the ruthenium atom and thiocyanate ligands, and the LUMOs possess π*(tcterpy) character with considerable carboxyl contribution. In the theoretically simulated absorption spectra, the first four bands are attributed to Ru/NCS→π*(tcterpy) charge-transfer (MLCT/LLCT) transitions, whereas the fifth one with the strongest intensity arises from intraligand tcterpy π→π* charge transfer (ILCT) mixed with some $O(p_z)$→terpy charge transfer (LLCT). Our calculations reveal that the MLCT/LLCT absorption bands in water are blue-shifted with respect to those in ethanol, agreeing with experimental observations. This can be rationalized by a decreased dipole moment in the excited state. The phosphorescent emissions are calculated to occur at 724, 711, and 691 nm in the gas phase, in ethanol, and in water, respectively, all with the same ^{3}LMCT/^{3}LLCT character.

1. Introduction

In recent years, dye-sensitized solar cells (DSSCs) have attracted considerable interest for the conversion of sunlight into electricity because of their low cost and high efficiency.[1–4] The DSSCs comprise four major parts: a nanocrystalline metal oxide semiconductor film, a dye sensitizer, a redox electrolyte, and a counter electrode. Undoubtedly, one of the key components of these cells is the dye sensitizer, which is used to sensitize the semiconductor electrode. An efficient solar cell sensitizer should fulfill several requirements: (1) it must be strongly adsorbed onto the semiconductor surface to ensure device stability and good electronic coupling for charge injection; (2) it should exhibit intense absorption in the visible part of the spectrum and form long-lived excited states with energies matching those of the conduction band of the semiconductor substrate;[3] (3) its redox potential should be sufficiently high, so that it can be regenerated rapidly by electron donation from the electrolyte or a hole conductor.

In the search for a promising sensitizer, a considerable number of complexes have been synthesized and analyzed.[4–10] Among these dyes, *cis*-dithiocyanatobis(2,2′-bipyridyl-4,4′-dicarboxylate)ruthenium(II) (hereafter referred to as N3 or red dye)[5] and trithiocyanato(4,4′,4′′-tricarboxy-2,2′:6′,2′′-terpyridine)ruthenium(II) (black dye)[6] are the most well-known. The N3 dye has been regarded as an efficient photosensitizer because of its broad range of visible light absorption, relatively long-lived excited states, and high thermal stability; moreover, the presence of terminal acidic carboxyl group allows stable anchoring of the dye to the semiconductor surface.[11–15] The incident photon to current conversion efficiency (IPCE) values are reported to be nearly 80% in the range 400–600 nm. However, the main drawback of this sensitizer is its lack of absorption in the red region of the visible spectrum. Numerous attempts to synthesize superior sensitizers[16–19] failed to improve the efficiency and to enhance the spectral response in the red and infrared region until 1997. In 1997, Grätzel and co-workers[20] reported a terpyridine–Ru^{II} complex, the "black dye", with visible absorption extending into the near-IR region up to 920 nm, yielding over 80% IPCE, and producing an overall efficiency of 10.4%.

Black dyes having different degrees of protonation have been fully characterized by Grätzel and co-workers.[6,20–22] It is conceived that the absorption spectra of the black dyes are dominated by metal-to-ligand-charge-transfer (MLCT) transitions. For example, the absorption spectrum of the

[a] State Key Laboratory of Theoretical and Computational Chemistry, Institute of Theoretical Chemistry, Jilin University, Changchun 130023, China
Fax: +86-431-88945942
E-mail: zhanghx@mail.jlu.edu.cn
[b] College of Chemistry and Chemical Engineering, Heilongjiang University,
Haerbin 150080, China

Supporting information for this article is available on the WWW under http://www.eurjic.org or from the author.

monoprotonated black dye complex (hereafter named **1H**) in ethanol exhibits three MLCT bands in the visible region centered at 610, 536, and 411 nm, and a high-energy $\pi\rightarrow\pi^*$ band at about 340 nm. It shows a strong negative solvatochromism, resulting in a red-shift of the UV/Vis absorption bands from 570 nm (in H_2O) to 620 nm (in γ-butyrolactone).[6] The observed emission of the complex **1H** (854 nm) has been assigned as arising from the Ru→tcterpy CT excited state.[6] Similarly, the emissions of the complex **1H** in different solvents also show a strong solvent dependence.

Since the spectroscopic properties of the dye are crucial in determining its long-term stability, the light-harvesting efficiency of the DSSCs, and the charge-transfer dynamics at the semiconductor interface,[16,23] a full understanding of its electronic properties, especially in the excited state, is very essential. In contrast to the numerous experimental studies, only a few theoretical calculations have been performed for dye molecules.[23–30] Most of these investigations are focused on the calculations of the N3 dye.[25–30] To date, one investigation for the fully protonated black dye is limited to the gas-phase calculations of molecular structure and absorption spectrum.[23] Another theoretical investigation focuses on the comparative study of ground-state properties (such as energies, geometries, and population analysis in molecular orbitals) and the absorption spectra of the black dye complex and its linkage isomers.[24] These theoretical calculations all focus on the fully protonated black dye complex. However, the photovoltaic performance of the monoprotonated black dye, **1H**, is superior to the other three black dye complexes. Moreover, no theoretical study was conducted on the geometry and electronic structure of the excited states and the emission properties of the black dye. In addition, in the solar cell, the dye sensitizer is adsorbed on the semiconductor electrode on one hand and interacts with the redox electrolyte on the other hand; therefore, it may not be possible to directly apply calculations excluding environment effects. Thus, in this paper, we employed DFT, the CIS method, and the TD-DFT approach to study the electronic structure, spectroscopic properties, and solvatochromic properties of the monoprotonated black dye **1H**. The solvent effects are seriously considered by using the conductor-like polarizable continuum model (CPCM). These results will provide a direct insight into the origins of the observed transitions and their possible role in dye–sensitized solar cell injection dynamics as well as the design of new and more efficient solar cell sensitizers.

2. Computational Details and Theory

In this work, C_s symmetry was adopted to set the conformation of $[Ru(Htcterpy)(NCS)_3]^{3-}$ (**1H**) in both the ground and the excited states. The geometry of the ground-state structure is fully optimized by using the density functional theory (DFT) with the B3LYP functional (Becke's three-parameter functional and the Lee–Yang–Parr functional),[31] while the geometry of the excited-state structure is fully optimized by the single-excitation configuration interaction (CIS) method.[32,33] With such calculations, the spectroscopic properties related to absorption and emission are obtained by the time-dependent density functional theory (TD-DFT),[34] and the conductor-like polarizable continuum model (CPCM)[35] is employed to account for the effects of the solvent molecules water and ethanol.

It is well-known that for excited states, the CIS method is most similar to the HF method for the ground state. However, through the use of analytic gradients and methods properly by including the effects of electronic correlation, this method gives bond lengths, frequencies, and dipole moments well in line with the experimental values. In addition, the application of the method to very large molecules is possible.[32] Although a reasonable excited-state structure can be obtained by the CIS method, the predicted transition energies deviate from experimental values commonly by about 1 eV or more. In the recent years, the TD-DFT methods have been successfully used to calculate singlet–singlet and singlet–triplet transitions in many reports.[36] More electronic correlations are involved in the TD-DFT (B3LYP) approach, which then yields more accurate excitation energies than the CIS method. This approach overcomes many of the problems encountered in vertical energies with the CIS method, providing accurate excitation energies of valence and Rydberg states. Therefore, on the basis of CIS optimized structures, we have employed the TD-DFT method to calculate the emission energies.

In the calculations, quasi-relativistic pseudopotentials of the Ru, C, N, and S atoms proposed by Hay and Wadt[37] with 16, 4, 5, and 6 valence electrons, respectively, are employed, and the LanL2DZ basis sets associated with the pseudopotential are adopted. Here, the basis sets are taken as Ru(8s7p6d/6s5p3d), S(3s3p1d/2s2p1d), N(10s5p/3s2p), C(10s5p/3s2p), and H(4s/2s). Thus, 361 basis functions and 262 electrons are included for the complex **1H**. All the calculations were accomplished by using the Gaussian (Revision B.03) program package[38] on an Origin/3900 server.

3. Results and Discussion

3.1 The Ground- and Excited-State Structures of 1H

The DFT optimization on **1H** indicates that the complex has a $^1A'$ ground state with the $[101(a'^2)30(a''^2)]$ electronic configuration. The geometry of the structure is depicted in Figure 1, and the main optimized geometry parameters in the gas phase are listed in Table 1 together with the X-ray crystal structure data of $(NBu_4^+)_2[Ru(H_2tcterpy)(NCS)_3]^{2-}$.[22] As shown in Figure 1, complex **1H** has a slightly distorted octahedral coordination with C_s symmetry. The geometry of the structure of complex **1H** displays a RuN6 central core derived from three nitrogen atoms of the terpyridine ligand and three nitrogen atoms of the isothiocyanate ligands. The coordination axis is also shown in Figure 1; the tcterpy-Ru-N1C1S1 moiety lies on the *xy* plane, and the other two isothiocyanate ligands are slightly tilted with respect to the *z* axis. As shown in Table 1,

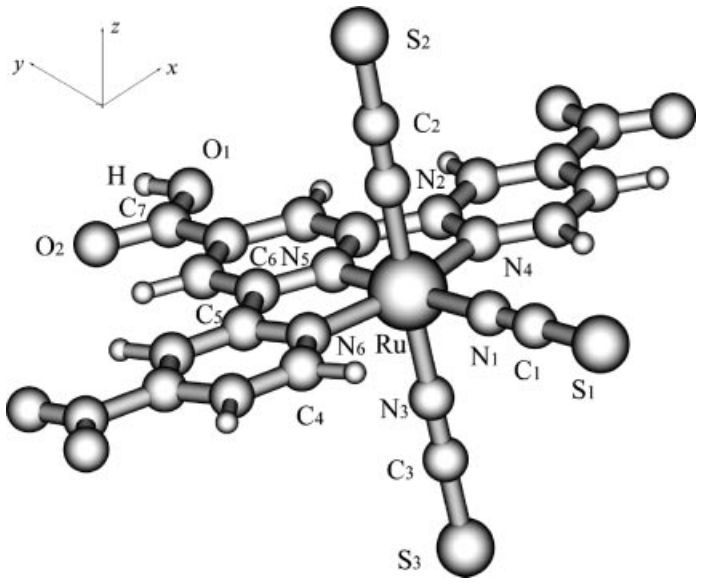

Figure 1. Ground-state structure of $[Ru(Htcterpy)(NCS)_3]^{3-}$ (**1H**) optimized by DFT(B3LYP).

the optimized geometrical parameters are in excellent agreement with the available X-ray data, and consistent with those calculated by Aiga and co-workers[23] by the PBE0 approach.[39] The N–C bond lengths in the terpyridine rings are about 1.38 Å and are much shorter than a normal N–C single-bond length of 1.48 Å, indicating that there is some delocalization of the lone pairs of the nitrogen atoms. It is noted that there exits an extended π bonding between the central pyridine (nitrogen p orbitals), the Ru atom (d π orbitals), and the N1C1S1 ligand (π electrons). The effective π bonding makes the bond lengths of Ru–N1 and Ru–N5 quite similar. Therefore, the Ru–N5 bond length (1.939 Å) is ca. 0.16 Å shorter than that of Ru–N4 (or Ru–N6), whereas the Ru–N1 bond length is ca. 0.05 Å longer than that of Ru–N2 (or Ru–N3). In addition to the bond lengths, the important bond angles are also accurately reproduced.

On the basis of the optimized ground-state structure, the CIS method is used to optimize the geometry of the excited-state structure of the **1H** complex, and the lowest-energy triplet excited state with $^3A'$ symmetry is obtained. The main geometry parameters of the excited state are presented in Table 1. Three conclusions can be drawn from the excited-state results: (1) The coordination geometry of Ru in the $^3A'$ excited state still keeps the quasi-octahedral structure similar to the ground state. (2) A general elongation of all the metal–ligand bonds is observed. For example, the Ru–N bond lengths in the excited state are elongated by ca. 0.04–0.07 Å relative to the ground-state ones. (3) The most nonmetallic bonds (N–C, C–C, C–O, and O–H) of tcterpy in the triplet excited state are shorter than those in the ground state, on the contrary, the C–S bond lengths for the NCS ligands are slightly longer upon excitation. It is noteworthy that the comparison of the bond lengths is between the ground state and the excited state obtained with two different methods (DFT/B3LYP for the ground state and CIS for the excited state). So the conclusions drawn from those comparisons are only used as relative results. However, this has no impact on the nature of the charge-transfer transition related to the emissions for the complex **1H**.

Table 1. Optimized geometry parameters for the $^1A'$ ground state calculated by DFT and for the $^3A'$ triplet excited state calculated by CIS for $[Ru(Htcterpy)(NCS)_3]^{3-}$ (**1H**), together with the experimental data.

Parameters	Ground state ($^1A'$)	Triplet excited state ($^3A'$)	Exp.[a]
Bond lengths [Å]			
Ru–N1	2.107	2.147	2.032
Ru–N2	2.057	2.098	2.052
Ru–N5	1.939	1.995	1.936
Ru–N6	2.099	2.174	2.090
N1–C1	1.192	1.159	
N2–C2	1.191	1.160	
N5–C6	1.382	1.354	
N6–C4	1.357	1.341	
N6–C5	1.384	1.365	
C1–S1	1.696	1.709	1.672
C2–S2	1.694	1.703	1.613
C7–O1	1.320	1.292	
H1–O1	0.982	0.954	
Bond angles [°]			
N6–Ru–N5	80.2	78.7	81.1
N6–Ru–N4	160.3	157.5	161.6
N2–Ru–N3	177.1	179.8	177.4
N1–Ru–N5	180.0	180.0	177.6
N1–Ru–N6	99.9	101.3	101.4
H1–O1–C7	109.8	113.5	

[a] Ref.[22]

3.2. Absorption Spectra

3.2.1. Electronic Structures

On the basis of the optimized ground-state geometry, the electronic structure of the excited state and the absorption

properties of **1H** in ethanol solution are obtained by the combination of the TD-DFT and CPCM methods. The frontier orbitals play a relevant role in complex **1H**, because they rule the electronic excitations and the transition character. The following assignment for each molecular orbital was made according to its composition (Table 2) and by visual inspection of its three-dimensional representation (e.g. Figure 2). Some lower-lying occupied molecular orbitals (such as 95a′, 26a′′, 96a′, and 27a′′) are centered on the carboxyl groups. The COO^- character of the lower-lying HOMOs was already found in the bipyridine–Ru^{II} complex by De Angelis et al.[40,41] The HOMO(30a′′) and HOMO-1(29a′′), lying within 0.02eV, are a set of quasi-degenerate orbitals arising from the antibonding combinations of ruthenium d orbitals (d_{xz} and d_{yz}, respectively) with sulfur p orbitals and nitrogen lone pairs of the two NCS ligands which are perpendicular to the tcterpy ring. HOMO-2(101a′), lying ca. 0.23 eV below the HOMO, is characterized by the antibonding combination nature between the ruthenium d_{xy} orbital and the NCS π orbital of the thiocyanate ligand that is in the plane of the tcterpy ligand. The HOMO-3(100a′) and HOMO-4(99a′), lying 0.46 and 0.47 eV below the HOMO, respectively, are mainly localized on the COO^- ligands which are attached to the peripheral pyridines, and have vanishing metal character. The HOMO-5(28a′′), HOMO-6(98a′), and HOMO-7(97a′), lying 0.51, 0.64, and 0.66 eV below the HOMO, respectively, are all pure NCS π orbitals. This significant thiocyanate character in the HOMOs was already found in the N3 dye[29,30] and seems to play an important role in the regeneration of dye-sensitized solar cells.[30]

The five lowest LUMOs of the **1H** complex, lying 1.92 eV above the HOMO within a range of ca. 1.86 eV, are π* orbitals localized over the pyridine ligands with considerable contributions arising from the carboxyl groups. In particular, the LUMO(31a′′) is localized on the central pyridine, while LUMO+3(34a′′) and LUMO+4(35a′′) are localized on the two peripheral pyridine groups. LUMO+1(32a′′) and LUMO+2(33a′′) are completely delo-

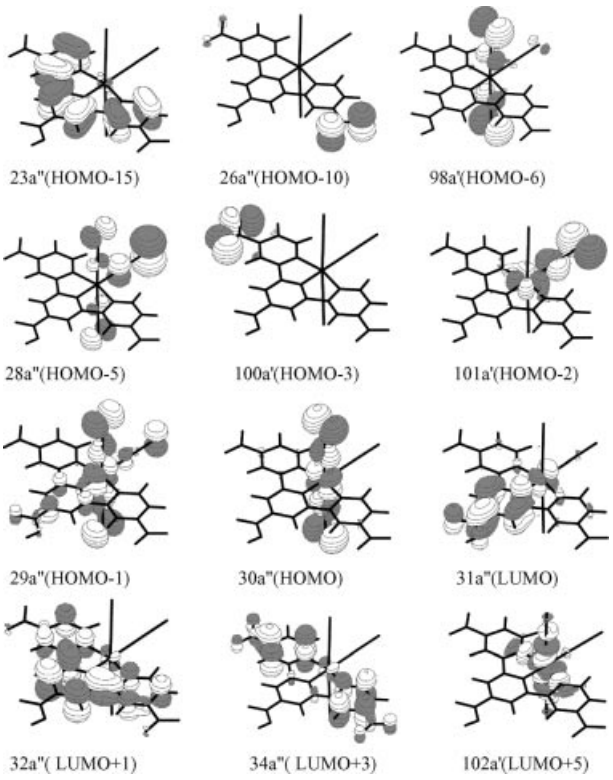

Figure 2. Electron-density diagrams of the frontier molecular orbitals involved in absorption for $[Ru(Htcterpy)(NCS)_3]^{3-}$ (**1H**) in ethanol calculated by TD-DFT.

Table 2. Partial molecular orbital compositions of $[Ru(Htcterpy)(NCS)_3]^{3-}$ (**1H**) in ethanol calculated by TD-DFT.

MO	Energy [eV]	Compositions [%]				Ru components [%]			Orbital assignment
		Ru	terpy	COO^-	NCS	s	p	d	
102a′	1.4727	44.5	26.5		28.3	5.8 s	3.2p_y	28.0 d_{z^2},7.5 $d_{x^2-y^2}$	$d_{z^2}/d_{x^2-y^2}$(Ru)-π*(NCS)
35a′′	0.1075		91.4	7.4					π*(tcterpy)
34a′′	–0.0215		89.8	6.9				3.2 d_{xz}	π*(tcterpy)
33a′′	–0.5646		76.6	21.5					π*(tcterpy)
32a′′	–1.0830		97.2						π*(tcterpy)
31a′′(L)	–1.7777	14.5	57.8	23.7	4.0			14.4 d_{yx}	π*(tcterpy)
30a′′(H)	–3.6970	40.6	5.1		53.9			40.6 d_{xz}	d_{xz} (Ru)–π*(NCS)
29a′′	–3.7160	30.5			49.8			29.9 d_{yz}	d_{yz} (Ru)–π*(NCS)
101a′	–3.9226	35.3			50.9			35.0 d_{xy}	d_{xy} (Ru)–π*(NCS)
100a′	–4.1549			81.4					$p_x/p_y(COO^-)$
99a′	–4.1656			81.4					$p_x/p_y(COO^-)$
28a′′	–4.2077				99.0				π*(NCS)
98a′	–4.3419				94.7				π*(NCS)
97a′	–4.3555				98.2				π*(NCS)
27a′′	–4.4447			98.2					$p_z(COO^-)$
96a′	–4.4458			62.3					$p_x/p_y(COO^-)$
26a′′	–4.4551			98.2					$p_z(COO^-)$
95a′	–4.4594			62.3					$p_x/p_y(COO^-)$
25a′′	–5.0224	43.5			35.8			43.5 d_{xz}	d_{xz}(Ru)–π*(NCS)
94a′	–5.0584	50.7			28.4			50.2 d_{xy}	d_{xy}(Ru)–π*(NCS)
24a′′	–5.2227	40.5			41.3			40.0 d_{yz}	d_{yz}(Ru)–π*(NCS)
23a′′	–5.8665		97.1						π(tcterpy)

calized over the full tcterpy ring ligands. Such a contribution from the carboxyl groups to the π* LUMOs should favor the electron injection process from the dye excited state to the semiconductor surface, because the carboxyl units serve as anchoring groups to the TiO_2 semiconductor surface.[2,3] Moreover, another role of the terminal carboxyl groups is to ensure intimate electronic coupling between the donor energy level of the excited dye and the acceptor TiO_2 conduction band.

3.2.2. Absorption Spectra in Ethanol

The absorption spectra of the complex **1H** are simulated with Gaussian curves based on the transitions with oscillator strength $f > 0$ in ethanol solution calculated by TD-DFT/CPCM. The fitting absorption curve is depicted as oscillator strength vs. wavelength in Figure 3; the most representative calculated optical transitions are collected in Table 3. Within the considered energy range, the absorption spectrum of **1H** shows five bands, labeled I, II, III, IV, and V in order of decreasing wavelength; band V is more intense than other bands.

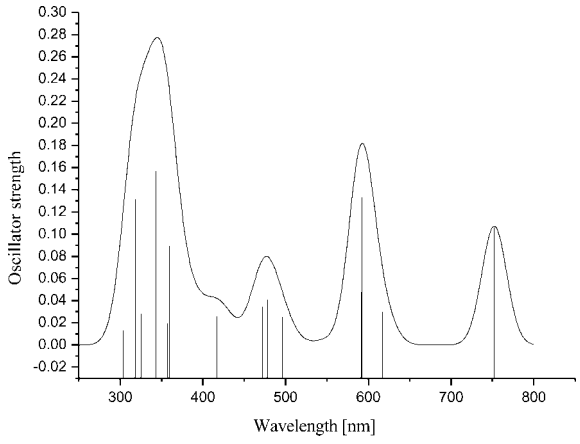

Figure 3. Absorption spectra and excited states of $[Ru(Htcterpy)(NCS)_3]^{3-}$ (**1H**) in ethanol calculated by TD-DFT.

The peak of the lowest-energy band, I, which results from one transition and has the oscillator strength 0.1073, is calculated to be at 752 nm. As shown in Table 3, the transition is mainly contributed by the excitations 29a′′(HOMO-1)→31a′′(LUMO) and 30a′′(HOMO)→32a′′(LUMO+1) with CI coefficients of ca. 0.58 and 0.25, respectively. It has been mentioned in the above section that the HOMO and HOMO-1 are antibonding combinations of the d orbitals ($d_{xz,yz}$) of the ruthenium atom with the π orbitals of the NCS ligand. The LUMO and LUMO+1 are π* orbitals localized over the tcterpy ring ligand. Therefore, we assign the lowest-energy band as a mixed Ru–NCS-to-tcterpy-charge-transfer (MLCT/LLCT) transition. The absorption band at 752 nm is not observed in the experimental absorption spectra. We calculated the maximum of band II to be at 592 nm, whose position is in excellent agreement with the experimental value of 610 nm. This band is caused by three transitions calculated at 617, 592, and 591 nm. As depicted in Table 2 and Table 3, band II is assigned as a mixed Ru–NCS-to-tcterpy charge transfer (MLCT/LLCT) with a little LMCT character. The dominating transition in this band, at 592 nm with an oscillator strength of 0.1300, is mainly contributed by the 28a′′(HOMO-5)→31a′′(LUMO) and 30a′′(HOMO)→32a′′(LUMO+1) configurations with CI coefficients of about 0.48 and 0.42, respectively. The molecular orbital 28a′′(HOMO-5) is localized on three NCS ligands up to 99% in composition, and the molecular orbital 31a′′(LUMO) is composed of $Ru(d_{yz})$ (15%), and tcterpy (82%). So we attribute the 592 nm absorption band to NCS→tcterpy charge transfer (LLCT), NCS→$Ru(d_{yz})$ charge transfer (LMCT), and $Ru(d_{xz})$→tcterpy charge transfer (MLCT) transitions. The maximum of band III is calculated at ca. 478 nm, which is only 58 nm blue-shifted with respect to the experimental datum of 536 nm, and has a multitransition character and involves excitations from the 25a′′(HOMO-12), 29a′′(HOMO-1), and 30a′′(HOMO) to the 31a′′(LUMO) and 33a′′(LUMO+2). This set of HOMOs have ruthenium-d-orbital nature (44%, 31%, and 41%, respectively) with sizeable contribution from the orbitals of the NCS ligand (36%, 50%, and 54%, respectively), while the LUMO and LUMO+2 are localized on the tcterpy ligands. Therefore, in the same way as for band I, the origin of band III is assigned to be the Ru–NCS to tcterpy charge transfer (MLCT/LLCT) transitions. Band IV, with the smallest oscillator strength, is calculated to have its maximum at 417 nm, which is in close accord with the experimental data of 411 nm. This band arises from one transition with a small oscillator strength of 0.0228, which mainly comes from the combination of 24a′′(HOMO-14)→31a′′(LUMO) and 30a′′(HOMO)→34a′′(LUMO+3) configurations with CI coefficients of around 0.50 and 0.42, respectively. In Table 2 and Figure 2, the 24a′′ orbital and 30a′′ orbital are both the antibonding combinations of Ru(d) orbitals and the NCS π orbitals, whereas the 31a′′ orbital and 34a′′ orbital are localized on tcterpy ring ligands. So the 417-nm band is unambiguously attributed to a mixed Ru–NCS to tcterpy charge transfer (MLCT/LLCT) transition. At the highest energy, the strongest band V, appears to be composed of multitransitions spanning the range 360–300 nm. The dominating transition in this band, at about 343 nm (f = 0.1536), is mainly contributed by the 23a′′(HOMO-15)→31a′′(LUMO) and 24a′′(HOMO-14)→32a′′(LUMO+1) configurations with CI coefficients of around 0.46 and 0.47, respectively. As show in Table 2 and Figure 2, we can see that the 23a′′ orbital (HOMO-15) and 31a′′ orbital (LUMO) are π combinations and π* combinations, respectively, localized on the tcterpy ligands. Thus the 343 nm absorption is attributed to the intraligand tcterpy π→π* charge transfer (ILCT) involved in a mixed Ru–NCS to tcterpy charge transfer (MLCT/LLCT) transition. The next most intense transition, at about 318 nm (f = 0.1283), arises from the combination of 25a′′(HOMO-12)→33a′′(LUMO+2), 26a′′(HOMO-10)→34a′′(LUMO+3), and 26a′′(HOMO-10)→35a′′(LUMO+4) configurations with CI coefficients of around 0.53, 0.32, and 0.21, respectively. The 25a′′ orbital (HOMO-12) is the anti-

Table 3. Excitation energies and oscillator strengths for the optical transitions with $f > 0.01$ for the absorptions of [Ru(Htcterpy)-$(NCS)_3]^{3-}$ (**1H**) in ethanol calculated by TD-DFT.

State	Excitation (CI coef.)	λ [nm] (E [eV])	Oscillator strength	Character
3A′	28a′′→31a′′(0.12)	752 (1.65)	0.1073	MLCT/LLCT
	29a′′→31a′′(0.58)			
	30a′′→32a′′(0.25)			
6 A′	29a′′→32a′′(0.69)	617 (2.01)	0.0268	MLCT/LLCT
9 A′	28a′′→31a′′(0.48)	592 (2.09)	0.1300	MLCT/LLCT/LMCT
	29a′′→31a′′(0.19)			
	30a′′→32a′′(0.42)			
10A′′	97a′→31a′′(0.70)	591 (2.10)	0.0443	LLCT/LMCT
16 A′	25a′′→31a′′(0.58)	496 (2.50)	0.0221	MLCT/LLCT
	30a′′→31a′′(0.13)			
	30a′′→33a′′(0.40)			
20 A′	25a′′→31a′′(0.37)	478 (2.60)	0.0375	MLCT/LLCT
	30a′′→33a′′(0.59)			
21 A′	29a′′→33a′′(0.68)	472 (2.63)	0.0310	MLCT/LLCT
32 A′	24a′′→31a′′(0.50)	417 (2.98)	0.0228	MLCT/LLCT
	30a′′→34a′′(0.42)			
46 A′	23a′′→31a′′(0.47)	360 (3.45)	0.0181	π→π*/MLCT/LLCT
	24a′′→32a′′(0.49)			
47 A′	24a′′→31a′′(0.27)	359 (3.45)	0.0864	MLCT/LLCT
	25a′′→32a′′(0.53)			
51 A′	26a′′→33a′′(0.66)	357 (3.47)	0.0164	$O(p_z)$→tcterpy
52 A′	23a′′→31a′′(0.46)	343 (3.61)	0.1536	π→π*/MLCT/LLCT
	24a′′→32a′′(0.47)			
57 A′	94a′→102a′(0.22)	325 (3.81)	0.0248	d→d/LLCT
	94a′→103a′(0.21)			
	101a′→102a′(0.41)			
	101a′→103a′(0.32)			
64 A′	25a′′→33a′′(0.25)	318 (3.90)	0.0125	$O(p_z)$→tcterpy/MLCT/LLCT
	26a′′→34a′′(0.39)			
	26a′′→35a′′(0.34)			
	27a′′→34a′′(0.32)			
66 A′	25a′′→33a′′(0.53)	318 (3.91)	0.1283	$O(p_z)$→tcterpy/MLCT/LLCT
	26a′′→34a′′(0.32)			
	26a′′→35a′′(0.21)			
70 A′	24a′′→33a′′(0.67)	304 (4.08)	0.0100	MLCT/LLCT

bonding combination of the Ru(d_{xz}) orbital and the NCS π orbitals, and the 26a′′ orbital (HOMO-10) is mainly composed of O(p_z) from the COO^- group. However, the 33a′′, 34a′′, and 35a′′ orbitals are all localized on tcterpy ligands. So the 318 nm transition is assigned as a mixed Ru–NCS-to-tcterpy charge transfer (MLCT/LLCT) and O(p_z)→terpy charge transfer (LLCT) transition. We also notice that a few weak (f = 0.0248) d–d transitions, at 325 nm, contribute to band V.

In experiments, the 610–400 nm regions have been assigned as the Ru-to-tcterpy-charge-transfer bands, while the 360–300 nm absorptions are attributed to the π→π* charge transfer transitions.[6] By comparing this experimental spectrum with the absorption spectrum of **1H** calculated in ethanol solution, we notice that our calculation is in rough agreement with experimental observations. However, there are some differences between the theoretical calculation and the experimental investigation. As mentioned above, we assign the low energy bands I–IV to mixed Ru–NCS-to-tcterpy charge transfer (MLCT/LLCT) rather than to pure metal–ligand-charge-transfer (MLCT) transitions, results from a set of Ru–NCS d-π* orbitals, while the highest energy band V, arises from intraligand tcterpy π→π* charge transfer (ILCT) and is involved in a sizeable O(p_z)→terpy charge transfer (LLCT) transition. Furthermore, the calculated absorption spectra have two peaks at long wavelengths around 600–800 nm, while the experimental spectra[6] have one peak. The calculated absorption peak at 752 nm is not observed in experiment. Moreover, the calculated absorption spectra have lesser intense bands at short wavelengths around 500–350 nm than those at longer wavelengths between 500–700 nm, but the experimental spectra have the reverse trend. Our calculation overestimates the intensity of band II (500–700) and underestimates that of band III (350–500 nm). This is perhaps not surprising, since from a comparison between TD-DFT and the more expansive CASPT2 method, the results of Full et al. show that TD-DFT oscillator strengths diverge from the CASPT2 values.[42] In addition, a similar comparison by Tozer et al. show that TD-DFT has difficulty distributing intensity properly;[43] it is thus possible that intensity is erroneously shifted from band III to band II in our calculation.

3.2.3. Solvent Effects

To check the solvent dependence of spectroscopic properties, we also calculated the absorptions of **1H** in the gas phase and in water solution, and the results are listed in Tables S1 and S2 (see Supporting Information). A compari-

son of the molecular orbital energy levels of the absorptions for complex **1H** in the gas phase, in ethanol and in water is presented in Figure 4. From Figure 4, we can see that the solvent effect leads to a sizeable change of the molecular orbital energies. However, the occupied and unoccupied orbitals maintain similar compositions in the gas phase and in solution (ethanol and water). In ethanol, the HOMOs (from HOMO to HOMO-7) are significantly stabilized by about 5.1 eV with respect to the corresponding values computed in the gas phase, while they maintain a similar composition. In the same way as the HOMOs, the five lowest LUMOs are stabilized by ca. 5.0–5.1 eV with respect to the corresponding values computed in the gas phase, even though they maintain similar compositions based on terpyridine and carboxyl group contributions. The LUMO+5 of the absorption in the gas phase has the C7–O1 π-bonding properties from the carboxyl group which is attached to the central pyridine, while in ethanol, the LUMO+5 orbital shows a higher contribution of d orbitals of the ruthenium atom (45%) mixed with π orbitals of the NCS ligand (28%). Altogether, the presence of the solvent leads to a slight increase of the HOMO–LUMO gap, which changes from 1.80 eV in the gas phase to 1.92 eV in ethanol. Moreover, the electronic structure of the absorption for complex **1H** in water is rather similar to that found in ethanol. The LUMOs and HOMOs are further stabilized, resulting in a HOMO–LUMO gap of 2.0 eV, namely 0.08 eV larger than that computed in ethanol.

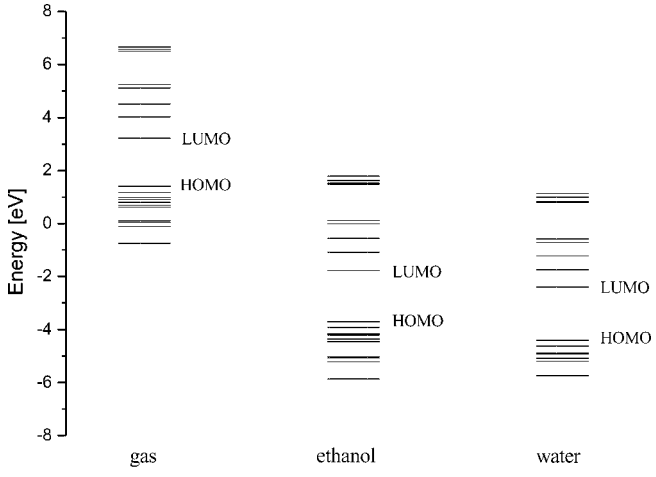

Figure 4. Energy-level diagrams of the orbitals involved in absorption for $[Ru(Htcterpy)(NCS)_3]^{3-}$ (**1H**) in the gas phase, in ethanol, and in water calculated by TD-DFT.

The calculated absorption spectra of complex **1H** in the gas phase, in ethanol and in water are shown in Figure 5. With the inclusion of seventy excitation states, all of these spectra exhibit five bands. As listed in Table 3 and Table S2, the CI configurations, oscillator strengths, and transition characters calculated in ethanol and water are rather similar. In both solvents, the four low-lying absorption bands have a mixed Ru–NCS-to-tcterpy charge transfer (MLCT/LLCT) character, whereas the high-lying absorption band V with the greatest intensity is attributed to the intraligand π→π* charge transfer mixed with $O(p_z)$→terpy charge transfer transitions. In the gas phase, the compositions of the transitions show a small variation relative to those in ethanol and water. As depicted in Table 2 and Table S1, we can see that the $O(p_z)$→terpy charge transfer character already appears in band VI in the gas phase. In the first two lowest-energy absorption bands, the wavelengths are blue-shifted by about 20 and 45 nm in ethanol and water with respect to those for the gas phase.

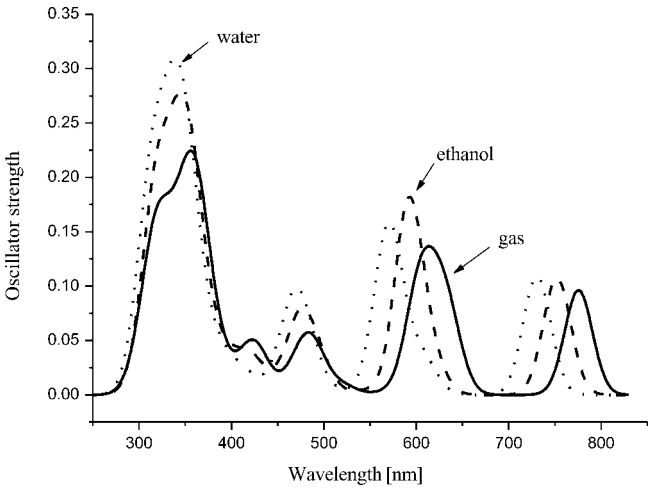

Figure 5. The simulated absorption spectra for $[Ru(Htcterpy)(NCS)_3]^{3-}$ (**1H**) in the gas phase, in ethanol, and in water.

As shown in Figure 5, negative solvatochromism is observed in the MLCT/LLCT band (λ = 400–800 nm) of complex **1H**. With increasing solvent polarity from ethanol to water, the wavelengths are blue-shifted by about 20 nm. In addition, we find that the π→π* band is only weakly affected by the change in solvent polarity. The calculated values are in excellent agreement with the experimental data. There is a factor that can be responsible for the observed blue-shift from ethanol to water: the electrostatic interaction between the solvent water and the NCS ligand is stronger than that between the solvent ethanol and the NCS ligand.

To get an insight into the origin of the negative solvatochromism of the MLCT/LLCT bands, it is useful to keep in mind the dipole moments of the complexes. As discussed above, the MLCT/LLCT transitions involve displacement of the electron charge from the Ru center and the NCS ligand toward the tcterpy π* orbitals. Thus, to approximately evaluate the dipole moment in the excited states, we considered the electronic state in which one electron is promoted from the HOMO(30a′′) to the LUMO(31a′′). The excited-state dipole moments in the gas phase, in ethanol and in water are predicted at the B3LYP/LAN2DZ level on the basis of the optimized ground-state geometry. Table S3 gives the dipole moments of complex **1H** in the ground and excited states in the gas phase, in ethanol, and in water. From Table S3, we can see that the dipole moments are apparently reduced from the ground state to the excited state. That is to say, the excited state should be less stabilized by polar solvents than the ground state. For instance,

in ethanol, the dipole moment in the excited state is 3.95 D, with a reduction $\Delta\mu$ = 5.81 D with respect to the dipole moment in the ground state (9.76 D). Similarly, in water, the dipole moment in the excited state is 2.96 D, with a reduction $\Delta\mu$ = 7.76 D with respect to the dipole moment in the ground state (10.72 D). The small increase in $\Delta\mu$ with increasing solvent polarity from ethanol to water correlates well with the calculated negative solvatochromism in the MLCT/LLCT band. It is noted that the definition of the dipole moment for neutral systems is independent of the choice of the origin of the reference system, while the dipole moment of charged systems will change as the molecule is shifted. However, in the present paper, the ground state and excited state exist as ions in the solvents. In addition, as discussed above, the excited-state dipole moments are predicted on the basis of the optimized ground-state geometry. So the center of coordinates of the ground and excited state do not change. Thus, though the complex **1H** is a charged molecule, we think it is reliable to discuss solvent effects in terms of the variation of dipole moment between the ground and excited states.

3.3. Emission Spectra

In view of obtaining a feasible emissive energy on the basis of the excited-state structures optimized by the CIS method, the emission spectrum of complex **1H** in ethanol is calculated by the TD-DFT approach at the B3LYP level associated with the CPCM model. The corresponding emissions of **1H** in the gas phase, in ethanol, and in water are listed in Table 4, associated with the emissive energies, transition assignments, and experimental values. To conveniently discuss the transition properties of the emissions, we present the partial compositions of the frontier molecular orbitals related to the emissions in Table 5.

The calculated lowest-energy emission for complex **1H** occurs at 711 nm in ethanol solution with a transition of $^3A'\rightarrow{}^1A'$ nature. As shown in Table 4, the phosphorescence is mainly from the transitions of 32a′′(LUMO+1)→24a′′(HOMO-14) and 32a′′(LUMO+1)→30a′′(HOMO) configuration with CI coefficients of 0.12 and 0.71, respectively. Furthermore, as seen in Table 4 and Table 5, this emission has tcterpy→Ru (^{3}LMCT) and tcterpy→NCS (^{3}LLCT)

Table 4. The lowest-energy phosphorescent emission of $[Ru(Htcterpy)(NCS)_3]^{3-}$ (**1H**) in the gas phase, in ethanol, and in water calculated by TD-DFT, together with experimental values.

Medium	Transition	Config.(CI coef.)	λ [nm] (E [eV])	Character	Exp.[a]
gas	$^3A'\rightarrow{}^1A'$	32a′′→24a′′(0.12) 32a′′→29a′′(0.16) 32a′′→30a′′(0.69)	724 (1.71)	^{3}LMCT/^{3}LLCT	
CH_3CH_2OH	$^3A'\rightarrow{}^1A'$	32a′′→24a′′(0.11) 32a′′→30a′′(0.71)	711 (1.74)	^{3}LMCT/^{3}LLCT	854
H_2O	$^3A'\rightarrow{}^1A'$	32a′′→24a′′(0.11) 32a′′→30a′′(0.71)	690 (1.80)	^{3}LMCT/^{3}LLCT	829

[a] From ref.[6]

Table 5. Partial molecular orbital compositions in the lowest-energy $^3A'$ excited state of $[Ru(Htcterpy)(NCS)_3]^{3-}$ (**1H**) in ethanol calculated by TD-DFT.

MO	Energy [eV]	Compositions [%]				Ru components [%]			Orbital assignment
		Ru	terpy	COO^-	NCS	s	p	d	
35a′′	0.1442		92.8	6.2					π*(terpy)
34a′′	–0.0063		90.9	6.4					π*(terpy)
33a′′	–0.4756		76.8	21.7					π*(terpy)
32a′′	–1.1889		98.0						π*(terpy)
31a′′(LUMO)	–1.7459	11.3	62.0	24.0	2.6			11.2 d_{yx}	π*(terpy)
30a′′(HOMO)	–3.6578	32.9	12.2		52.7			32.4 d_{yz}	d_{yz} (Ru)–π*(NCS)
29a′′	–3.6698	40.3			55.8			40.3 d_{xz}	d_{xz} (Ru)–π*(NCS)
101a′	–3.8499	34.9			52.8			34.7 d_{xy}	d_{xy} (Ru)–π*(NCS)
28a′′	–4.1098				99.6				π*(NCS)
100a′	–4.1490			80.8					$p_x/p_y(COO^-)$
99a′	–4.1615			80.8					$p_x/p_y(COO^-)$
98a′	–4.2230				94.7				π*(NCS)
97a′	–4.2330				98.2				π*(NCS)
96a′	–4.4409		38.0	61.5					$p_x/p_y(COO^-)$
95a′	–4.4562		38.0	61.5					$p_x/p_y(COO^-)$
27a′′	–4.4771			98.1					$p_z(COO^-)$
26a′′	–4.4894			98.1					$p_z(COO^-)$
94a′	–4.8562	53.1			26.9			52.7 d_{xy}	d_{xy}(Ru)–π*(NCS)
25a′′	–5.9095	51.0			34.4			51.0 d_{xz}	d_{xz}(Ru)–π*(NCS)
24a′′	–5.0747	47.8	12.1		38.6			47.3 d_{yz}	d_{yz}(Ru)–π*(NCS)

character. The electron density diagrams of the frontier molecular orbitals for the 711 nm emission in Figure 6 provide intuitive evidence for the above assignment. As shown in Table 5 and Figure 6, the electron density mainly focuses around the tcterpy ligands: about 98% in the 32a′′(LUMO+1) orbital. The 24a′′(HOMO-14) and 30a′′(HOMO) orbitals are both composed of Ru^{II} and NCS ligands. The former is composed of 48% Ru(d_{yz}), 39% NCS ligands, and 12% tcterpy ligand, while the latter comprises 33% Ru(d_{yz}), 53% NCS ligands, and 12% tcterpy ligands.

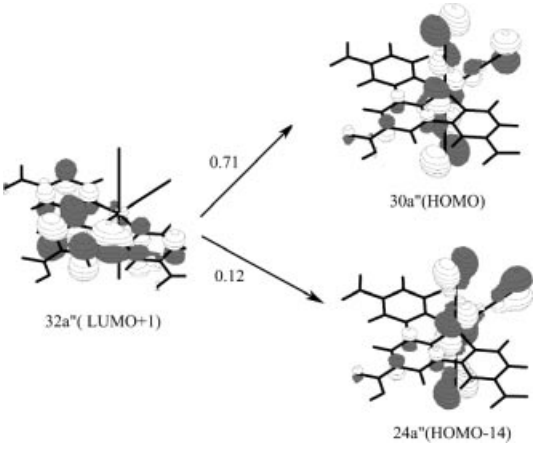

Figure 6. Single-electron transitions with |CI coefficient| > 0.1 calculated by TD-DFT for the 711-nm emission of $[Ru(Htcterpy)(NCS)_3]^{3-}$ (**1H**) in ethanol.

On the basis of the optimized $^3A'$ excited state, the 724- and 691-nm phosphorescence in the gas phase and in water solution are calculated by the TD-DFT method and the TD-DFT/CPCM method, respectively; these bands also have tcterpy→Ru/NCS-charge-transfer (^{3}LMCT/^{3}LLCT) character. The electron density diagrams of the frontier molecular orbitals related to the 724- and 691-nm emissions displayed in Figures S1–S2 can help us intuitively understand the nature of the transitions causing the emissions. The emission spectroscopic data of complex **1H** calculated in ethanol and water solution show a certain solvent dependence. In water, the emission maximum is blue-shifted (20 nm) relative to that in ethanol solution, because the electrostatic interaction between the solvent water and the NCS ligand is stronger than that between the solvent ethanol and the NCS ligand.

4. Conclusions

The electronic structure and spectroscopic properties of $[Ru(Htcterpy)(NCS)_3]^{3-}$ (**1H**) are investigated theoretically. We predict absorption and emission spectra in the gas phase and in solution by using the TD-DFT method without and with the solvent-effect CPCM model, respectively. The analysis of electronic structure in ethanol solution shows that the HOMOs are composed of d orbitals of the ruthenium atom and the thiocyanate ligands and the LUMOs are the admixture of π* orbitals localized on the terpyridine ring ligand and the carboxyl groups. The contributions of the thiocyanate and carboxyl group to the HOMOs and LUMOs, respectively, are believed to play an important role in the regeneration and electron-injection performance of dye-sensitized TiO_2 solar cells.

The calculated absorption spectra in ethanol solution are in rough agreement with the experimental data. The theoretically simulated spectra based on TD-DFT calculations contain four intense peaks and a shoulder. The calculated absorption peak at 752 nm is not observed in experiment. We assign four lower-energy bands as d(Ru) and NCS-to-tcterpy-charge-transfer (MLCT and LLCT) transitions, different from a previous assignment of pure MLCT transitions.[6] The fifth absorption band with the greatest intensity is attributed to a π→π* transition localized on the tcterpy ligand mixed with some O(p_z)→tcterpy charge transfer. Furthermore, our calculation overestimates the intensity of band II and underestimates that of band III.

To explore the effect of solvents on the spectra, we also calculated the absorptions of **1H** in the gas phase and in solution. The results quantitatively reproduce the negative solvatochromism (the MLCT/LLCT electronic transition energies of complex **1H** decrease upon increasing solvent polarity). We find that the MLCT/LLCT absorption bands are blue-shifted by about 20 nm in going from ethanol solvent to water solvent. The appearance of negative solvatochromism is closely related to a negative change of dipole moment in the excited state with respect to the ground state, which results in a higher stabilization of the ground state in solvents with increasing polarity.

TD-DFT predicts phosphorescent emissions at 724, 711, and 691 nm in the gas phase, in ethanol, and in water, respectively. We attribute them to tcterpy→Ru/NCS charge transfer (^{3}LMCT/^{3}LLCT) transitions.

Supporting Information (see footnote on the first page of this article): Figures S1 and S2 are the diagrams of the single-electron transitions for the emissions in the gas phase and in water solution, respectively. Tables S1 and S2 present the calculated absorptions of **1H** in the gas phase and in water. The calculated dipole moments of the ground and excited states of **1H** in the gas phase, in ethanol, and in water are given in Table S3.

Acknowledgments

This work is supported by the Natural Science Foundation of China (20173021, 20333050, and 20573042).

[1] B. O'Regan, M. Grätzel, *Nature* **1991**, *353*, 737–740.
[2] A. Hagfeldt, M. Grätzel, *Acc. Chem. Res.* **2000**, *33*, 269–277.
[3] M. Grätzel, *Nature* **2001**, *414*, 338–344.
[4] K. Kalyanasundaram, M. Grätzel, *Coord. Chem. Rev.* **1998**, *177*, 347–414.
[5] M. K. Nazeeruddin, A. Kay, I. Rodicio, R. Humphry-Baker, E. Müeller, P. Liska, N. Vlachopoulos, M. Grätzel, *J. Am. Chem. Soc.* **1993**, *115*, 6382–6390.
[6] M. K. Nazeeruddin, P. Péchy, T. Renouard, S. M. Zakeeruddin, R. Humphry-Baker, P. Comte, P. Liska, L. Cevey, E. Costa, V. Shklover, L. Spiccia, G. B. Deacon, C. A. Bignozzi, M. Grätzel, *J. Am. Chem. Soc.* **2001**, *123*, 1613–1624.

[7] S. M. Zakeeruddin, M. K. Nazeeruddin, R. Humphry-Baker, P. Péchy, P. Quagliotto, C. Barolo, G. Visvardi, M. Grätzel, *Langmuir* **2002**, *18*, 952–954.
[8] M. K. Nazeeruddin, F. D. Angelis, S. Fantacci, A. Selloni, G. Viscardi, P. Liska, S. Ito, B. Taleru, M. Grätzel, *J. Am. Chem. Soc.* **2005**, *127*, 16835–16847.
[9] Z.-S. Wang, T. Yamaguchi, H. Sugihara, H. Arakawa, *Langmuir* **2005**, *21*, 4272–4276.
[10] C. Barolo, M. K. Nazeeruddin, S. Fantacci, D. D. Censo, P. Comte, P. Liska, G. Viscard, P. Quagliotto, F. D. Angelis, S. Ito, M. Grätzel, *Inorg. Chem.* **2006**, *45*, 4642–4653.
[11] V. Shklover, M. K. Nazeeruddin, S. M. Zakeeruddin, C. Barbè, A. Kay, T. Haibach, W. Steurer, R. Hermann, H.-U. Nissen, M. Grätzel, *Chem. Mater.* **1997**, *9*, 430–439.
[12] V. Shklover, Yu. E. Ovchinnikov, L. S. Graginsky, S. M. Zakeeruddin, M. Grätzel, *Chem. Mater.* **1998**, *10*, 2533–2541.
[13] M. K. Nazeeruddin, S. M. Zakeeruddin, R. Humpry-Baker, S. I. Gorelsky, A. B. P. Lever, M. Grätzel, *Coord. Chem. Rev.* **2000**, *208*, 213–225.
[14] Md. K. Nazeeruddin, S. M. Zakeeruddin, R. Humpry-Baker, M. Jirousek, P. Liska, N. Vlachopoulos, V. Shklover, C.-H. Fisher, M. Grätzel, *Inorg. Chem.* **1999**, *38*, 6298–6305.
[15] S. M. Zakeeruddin, Md. K. Nazeeruddin, R. Humpry-Baker, M. Grätzel, *Inorg. Chim. Acta* **1999**, *296*, 250–253.
[16] M. K. Nazeeruddin, E. Muller, R. Humphry-Baker, N. Vlachopoulos, M. Grätzel, *J. Chem. Soc., Dalton Trans.* **1997**, *23*, 4571–4578.
[17] S. M. Zakeeruddin, M. K. Nazeeruddin, P. Pechy, F. P. Rotzinger, R. Humphry-Baker, K. Kalyanasundaram, M. Grätzel, V. Shklover, T. Haibach, *Inorg. Chem.* **1997**, *36*, 5937–5946.
[18] S. Ruile, O. Kohle, P. Péchy, M. Grätzel, *Inorg. Chim. Acta* **1997**, *261*, 129–140.
[19] C. Klein, M. K. Nazeeruddin, P. Liska, D. D. Censo, N. Hirata, E. Palomares, J. R. Durrant, M. Grätzel, *Inorg. Chem.* **2005**, *44*, 178–180.
[20] M. K. Nazeeruddin, P. Péchy, M. Grätzel, *Chem. Commun.* **1997**, 1705–1706.
[21] Y. V. Zubavichus, Y. L. Slovokhotov, M. K. Nazeeruddin, S. M. Zakeeruddin, M. Grätzel, V. Shklover, *Chem. Mater.* **2002**, *14*, 3556–3563.
[22] V. Shklover, M. K. Nazeeruddin, M. Grätzel, Y. E. Ovchinnikov, *Appl. Organomet. Chem.* **2002**, *16*, 635–642.
[23] F. Aiga, T. Tada, *J. Mol. Struct.* **2003**, *658*, 25–32.
[24] S. Ghosh, G. K. Chaitanya, K. Bhanuprakash, M. K. Nazeeruddin, M. Grätzel, P. Y. Reddy, *Inorg. Chem.* **2006**, *45*, 7600–7611.
[25] H. Rensmo, S. Södergren, L. Patthey, K. Westmark, L. Vayssieres, O. Khole, P. A. Brühwiler, A. Hagfeldt, H. Siegbahn, *Chem. Phys. Lett.* **1997**, *274*, 51–57.
[26] F. Cecchet, A. M. Gioacchini, M. Marcaccio, F. Paolucci, S. Roffia, M. Alebbi, C. A. Bignozzi, *J. Phys. Chem. B* **2002**, *106*, 3926–3932.
[27] A. Broo, P. Lincoln, *Inorg. Chem.* **1997**, *36*, 2544–2553.
[28] S. I. Gorelsky, E. S. Dodsworth, A. B. P. Lever, A. A. Vlcek, *Coord. Chem. Rev.* **1998**, *174*, 469–494.
[29] J. E. Monat, J. H. Rodriguez, J. K. McCusker, *J. Phys. Chem. A* **2002**, *106*, 7399–7406.
[30] S. Fantacci, F. D. Angelis, A. Selloni, *J. Am. Chem. Soc.* **2003**, *125*, 4381–4387.
[31] A. D. Becke, *J. Chem. Phys.* **1993**, *98*, 5648–5652.
[32] a) J. F. Stanton, J. Gauss, N. Ishikawa, M. Head-Gordon, *J. Chem. Phys.* **1995**, *103*, 4160–4174; b) J. B. Foreman, M. Head-Gordon, A. Pople, *J. Phys. Chem.* **1992**, *96*, 135–149; c) V. A. Waiters, C. M. Hadad, Y. Thiel, S. D. Colson, K. B. Wibergy, P. M. Johnson, J. B. Foresmanl, *J. Am. Chem. Soc.* **1991**, *113*, 4782–4791.
[33] a) H. X. Zhang, C. M. Che, *Chem. Eur. J.* **2001**, *7*, 4887–4893; b) Q. J. Pan, H. X. Zhang, *J. Chem. Phys.* **2003**, *119*, 4346–4352; c) Q. J. Pan, H. X. Zhang, *J. Phys. Chem. A* **2004**, *108*, 3650–3661; d) Q. J. Pan, H. X. Zhang, *Eur. J. Inorg. Chem.* **2003**, 4202–4210; e) Q. J. Pan, H. X. Zhang, *Inorg. Chem.* **2004**, *43*, 593–601.
[34] a) M. E. Casida, C. Jamorski, K. C. Casida, D. R. Salahub, *J. Chem. Phys.* **1998**, *108*, 4439–4449; b) R. E. Stratmann, G. E. Scuseria, *J. Chem. Phys.* **1998**, *109*, 8218–8224; c) N. N. Matsuzawa, A. Ishitani, *J. Phys. Chem. A* **2001**, *105*, 4953–4962.
[35] a) V. Barone, M. Cossi, *J. Phys. Chem. A* **1998**, *102*, 1995–2001; b) M. Cossi, N. Rega, G. Scalmani, V. Barone, *J. Comput. Chem.* **2003**, *24*, 669–681.
[36] a) R. Bauernschmitt, R. Ahlrichs, *Chem. Phys. Lett.* **1996**, *256*, 454–464; b) A. Rosa, E. J. Baerends, S. J. A. V. Gisbergen, E. Lenthe, J. A. Groeneveld, J. G. Snijders, *J. Am. Chem. Soc.* **1999**, *121*, 10356–10365.
[37] a) W. R. Wadt, P. J. Hay, *J. Chem. Phys.* **1985**, *82*, 284–298; b) P. J. Hay, W. R. Wadt, *J. Chem. Phys.* **1985**, *82*, 299–310.
[38] M. J. Frisch, G. W. Trucks, H. B. Schlegel, G. E. Scuseria, M. A. Robb, J. R. Cheeseman, J. A. Montgomery Jr, T. Vreven, K. N. Kudin, J. C. Burant, J. M. Millam, S. S. Iyengar, J. Tomasi, V. Barone, B. Mennucci, M. Cossi, G. Scalmani, N. Rega, G. A. Petersson, H. Nakatsuji, M. Hada, M. Ehara, K. Toyota, R. Fukuda, J. Hasegawa, M. Ishida, T. Nakajima, Y. Honda, O. Kitao, H. Nakai, M. Klene, X. Li, J. E. Knox, H. P. Hratchian, J. B. Cross, C. Adamo, J. Jaramillo, R. Gomperts, R. E. Stratmann, O. Yazyev, A. J. Austin, R. Cammi, C. Pomelli, J. W. Ochterski, P. Y. Ayala, K. Morokuma, G. A. Voth, P. Salvador, J. J. Dannenberg, V. G. Zakrzewski, S. Dapprich, A. D. Daniels, M. C. Strain, O. Farkas, D. K. Malick, A. D. Rabuck, K. Raghavachari, J. B. Foresman, J. V. Ortiz, Q. Cui, A. G. Baboul, S. Clifford, J. Cioslowski, B. B. Stefanov, G. Liu, A. Liashenko, P. Piskorz, I. Komaromi, R. L. Martin, D. J. Fox, T. Keith, M. A. Al-Laham, C. Y. Peng, A. Nanayakkara, M. Challacombe, P. M. W. Gill, B. Johnson, W. Chen, M. W. Wong, C. Gonzalez, J. A. Pople, *Gaussian 03*, Revision B.03, Gaussian, Inc., Pittsburgh, PA, **2003**.
[39] C. Adamo, G. E. Scuseria, V. Barone, *J. Chem. Phys.* **1999**, *111*, 2889–2899.
[40] F. De Angelis, S. Fantacci, A. Selloni, *Chem. Phys. Lett.* **2004**, *389*, 204–208.
[41] F. De Angelis, S. Fantacci, A. Selloni, M. L. Nazeeruddin, *Chem. Phys. Lett.* **2005**, *415*, 115–120.
[42] J. Full, L. Gonzalez, C. Daniel, *J. Phys. Chem. A* **2001**, *105*, 184–189.
[43] D. J. Tozer, R. D. Amos, N. C. Handy, B. O. Roos, L. Serrano-Andres, *Mol. Phys.* **1999**, *97*, 859–868.

Received: November 10, 2006
Published Online: April 10, 2007

